THE JOURNAL OF PHYSICAL CHEMISTRY C

Article

pubs.acs.org/JPCC

Modification of the Electrochemical Properties of Nile Blue through Covalent Attachment to Gold As Revealed by Electrochemistry and SERS

Andrew J. Wilson, Natalia Y. Molina, and Katherine A. Willets*

Department of Chemistry, Temple University, Philadelphia, Pennsylvania 19122, United States

Supporting Information

ABSTRACT: Conventional electrochemistry and surface-enhanced Raman scattering (SERS) spectroelectrochemistry are used to probe the redox reaction of Nile Blue immobilized on gold electrodes. Covalent attachment of Nile Blue (NB) to gold through carbodiimide cross-linking shows the appearance of a second, new redox reaction, unobserved by solution phase or physisorbed NB. Each redox reaction is characterized by differential pulse voltammetry to reveal two individual one-proton, one-electron electrochemical reactions. SERS spectroelectrochemistry along with electrochemical characterization of structurally similar Cresyl Violet are used to assign the electrochemical (de)protonation of the terminal amine and phenoxazine nitrogen to the lower and higher energy redox reactions, respectively. Analysis of covalently bound NB via azide–alkyne click chemistry supports the hypothesis that the electron-withdrawing carbonyl formed during the carbodiimide cross-linking induces a change in the electronic structure of NB, causing a shift in the terminal amine redox reaction to lower energy.

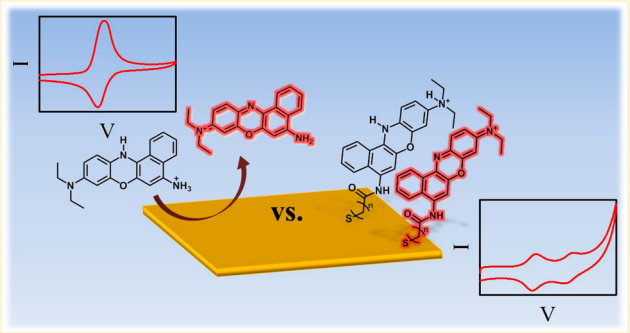

INTRODUCTION

As electrochemistry moves to the nanoscale, measuring current from the small number of molecules that interact with the electrode surface becomes increasingly difficult. To probe how nanoscale electrodes and subensemble populations of molecules behave on this length scale, methods that measure changes in charge transfer need to be expanded beyond conventional techniques such as voltammetry and amperometry. One possibility is to use optical measurements of electrochemical reactions, in which a spectroscopic signal, such as fluorescence or Raman scattering, changes in response to an electrochemical event.[1−11] One challenge with this strategy, however, is the limited number of probes that undergo changes in optical activity upon a change in their redox state. Although several optically active redox probes have been identified, the candidates that allow for single-molecule detection typically have highly conjugated pi electron systems that often undergo complex electrochemistry involving the transfer of many electrons and protons.[2,4,12−19] More ideal electrochemical probes that involve a one-electron transfer reaction typically either have weak optical signatures or require organic solvents to access the high overpotentials needed for electron transfer.[11] As a result, identifying and characterizing a simple electrochemical system based on optical readouts to probe the fundamentals of nanoelectrochemistry is an ongoing area of research.

Nile Blue (NB) is a key member in a class of phenoxazine dye molecules that are water-soluble and electrochemically addressable within the water potential window. In its oxidized form, NB gives a strong surface-enhanced Raman scattering (SERS) signature that permits single-molecule detection.[4,20] NB undergoes a two-proton, two-electron reduction (for pH < 6) to become nonemissive under visible-light excitation, satisfying the criterion of correlated optical and electrochemical modulation.[21] For example, Salvarezza and co-workers physisorbed NB onto Ag colloids and monitored electrochemical reduction and oxidation events from single molecules as the SERS signal modulated between a nonemissive and emissive state, respectively.[4] Interestingly, when individual redox events were histogrammed, the bulk voltammogram was not recovered from the single-molecule data. In addition, Salvarezza and co-workers have shown that the orientation of NB relative to the electrode surface can affect its redox potentials.[22] In another example, Ren and co-workers used transient electrochemical measurements to study fast electrochemical dynamics of NB when adsorbed to Ag colloids.[23] During cathodic scans, NB showed a surprising increase in the SERS intensity before the expected decrease, which was described as NB aggregate dissociation leading to an intensity rise, followed by electrochemical reduction resulting in the expected intensity fall. In our research using NB, we applied potential-dependent superlocalization microscopy to low

Special Issue: Richard P. Van Duyne Festschrift

Received: April 19, 2016
Revised: May 31, 2016
Published: May 31, 2016

DOI: 10.1021/acs.jpcc.6b03962
J. Phys. Chem. C 2016, 120, 21091−21098

concentrations of NB molecules adsorbed onto Ag colloids to reveal that the position of a NB molecule on a plasmonic nanoscale electrode determines, in part, the potential at which it is reduced and oxidized.[6]

All of the aforementioned experiments highlight important and novel behaviors of nanoelectrochemistry using physisorbed NB as a spectroelectrochemical probe but suffer from the possibility of desorption of the probe during the experiment or translation of the probe along the nanoparticle surface.[6] To prevent these problems, NB can be covalently attached to the electrode surface, thereby enabling interrogation of the effects of local electrode structure and environment on nanoelectrochemistry.[24,25] Recent work from our group probed NB electrochemistry using SERS from molecules covalently immobilized on spherical gold nanoparticles.[24] In this system, we observed anomalous SERS behaviors that did not follow the straightforward on/off optical modulation seen with physisorbed molecules, suggesting that the electrochemical properties of the dye were modified upon covalent attachment to the gold electrode surface. In this article, we investigate how covalent attachment of NB to gold electrodes affects both the electrochemical and SERS properties of the molecule, and we reveal that through the proper selection of linkage moieties, the electrochemical redox reaction of the tethered probe is simplified to one-electron and one-proton transfer reactions.

EXPERIMENTAL METHODS

Electrode Preparation. Gold disc electrodes (2 mm diameter) used for solution-based electrochemical measurements were polished with alumina powder (1.0 μm, 0.3 μm, 0.05 μm, CH Instruments) followed by sonication in nanopure water (18 MΩ·cm) for 60 s prior to use. Gold electrodes supported by indium tin oxide (ITO) were prepared by thermal evaporation. First, ITO-coated glass coverslips (15−30 Ω, SPI Supplies) were sonicated in acetone, 2-propanol, and nanopure water for 15 min in each solvent. Next, gold (99.95%, Ted Pella, Inc.) was thermally evaporated (Nano 36, Kurt J. Lesker) onto the cleaned ITO surface at a rate of 0.5 Å/s to a final thickness of 100 nm. A film thickness of 7 nm was used for spectroelectrochemical measurements to preserve substrate transparency and provide plasmonic enhancement of the optical signals. All ITO@Au samples were either used immediately or stored in vacuum before use to ensure cleanliness. A stable cyclic voltammogram was achieved after three potential cycles in sulfuric acid, indicating that our electrode preparation method produces an uncontaminated surface for chemical attachment (Figure S1). After electrode functionalization, a tinned-copper wire was attached to the ITO with silver epoxy (MG Chemicals) to serve as a lead for electrical contact.

Surface Tethering with EDC/NHS. A self-assembled monolayer (SAM) was formed on gold-coated ITO electrodes by immersion in a 10 mM ethanolic solution of 8-mercaptooctanoic acid (8MOA, Sigma-Aldrich) for 48 h. A surface coverage of 1×10^{-7} mol/cm^2 was determined by $\Gamma = Q/nFA$, where Q was calculated by integrating the desorptive reduction peak of 8MOA (Figure S2), n is the number of electrons (1), F is Faraday's constant, and A is the electrode area (0.02 cm^2).[26] After assembly, the electrodes were rinsed with ethanol and nanopure water and dried with nitrogen. The terminal carboxylic acid groups were then activated by incubation in 0.02 M 1-ethyl-3-(3-dimethylaminopropyl)-carbodiimide hydrochloride (EDC, Sigma-Aldrich) and 0.04 M *N*-hydroxysulfosuccinimide (NHS, Sigma-Aldrich) for 1 h. Excess EDC and NHS were removed by rinsing the electrodes with nanopure water. Finally, the NHS-activated electrodes were incubated in a solution of 10 μM Nile Blue A perchlorate (NB, Sigma-Aldrich) or Cresyl Violet acetate (Sigma-Aldrich) in 0.1 M phosphate buffer at pH 5 for 2 h. To remove unreacted NB or Cresyl Violet, the samples were rinsed profusely with acetone and nanopure water. Samples prepared in this way are referred to as EDC/NHS coupled NB.

Surface Tethering with Click Chemistry. (*S*)-(4-Azidobutyl)thioacetate (Sigma-Aldrich) was deprotected from the acetate according to the Sigma-Aldrich procedure. (*S*)-(4-Azidobutyl)thioacetate (0.5 g) was dissolved in 10 mL of ethanol and transferred to a 50 mL round-bottom flask in a nitrogen atmosphere. Eighteen mmol of NaOH (aq) (Sigma-Aldrich) was added to the reaction vessel dropwise. The mixture was then refluxed for 2 h. After the reaction, the solution was neutralized with 6 mL of 2 M HCl (Sigma-Aldrich) and transferred to a separatory funnel. Twenty milliliters of diethyl ether and 10 mL of water were added to the funnel, mixed, and separated. The remaining organic solvent was dried with Na_2SO_4 (Sigma-Aldrich) and evaporated. The final product was dissolved in 15 mL of ethanol and incubated over gold-coated ITO electrodes for 48 h to form an azide-terminated alkanethiol SAM.

After SAM formation, the electrodes were rinsed with ethanol and nanopure water. A solution was prepared containing 10 mL of 27 μM 625-Nile Blue Alkyne (NBA, Active Motif) in dimethyl sulfoxide and 10 mL of an aqueous solution of 20 mM ascorbic acid (Sigma-Aldrich) and 10 mM $CuSO_4 \cdot 5H_2O$ (Sigma-Aldrich). The final mixture was incubated over the electrodes in the dark on an orbital shaker overnight to allow reaction of the azide and alkyne moieties. Unreacted NBA was removed by rinsing the electrodes profusely with acetone and nanopure water. Samples prepared in this way are referred to as click-coupled NB.

Electrochemical Measurements. A 650E CH Instruments potentiostat was used to conduct all electrochemical and spectroelectrochemical measurements. Each experiment used a large surface area platinum wire as an auxiliary electrode and a Ag/AgCl (1 M KCl) reference electrode. A scan rate between 10 mV/s and 100 mV/s was used for cyclic voltammetry (CV). Differential pulse voltammetry (DPV) was performed using pulses with amplitudes of 50 mV lasting 50 ms over a 500 ms period (Figure S3). The voltammograms measured over 30 cycles are stable, indicating that no film damage occurs within the potential window in which we are operating.

Optical Methods. Spectroelectrochemical cells were prepared by attaching four glass slides to the top of the gold-coated ITO electrodes with clear epoxy (Devcon, Figure S4). The cells were then mounted on an Olympus IX-71 inverted microscope, filled with phosphate buffer, and connected to the potentiostat. A 642 nm laser was circularly polarized and focused to the back focal plane of a 20× objective for wide field excitation at the sample plane. SERS emission was collected with the same objective, passed through a dichroic and long pass filter, and then split between a Princeton Instruments ProEM 512 electron-multiplied charge-coupled device (EM-CCD) camera for imaging and a Princeton Instruments IsoPlane SCT320 spectrometer equipped with a ProEM 1600 EM-CCD for spectroscopy using a 50/50 beam splitter. Image integration was 200 ms. Spectral integration was 1 s for EDC/NHS coupled NB and 0.5 s for click coupled NB. Data

DOI: 10.1021/acs.jpcc.6b03962
J. Phys. Chem. C 2016, 120, 21091−21098

acquisition for each detector was synchronized with the potentiostat.

RESULTS AND DISCUSSION

The electrochemical redox reaction of NB in solution has previously been described as a two-proton, two-electron transfer process in acidic conditions and a one-proton, two-electron transfer process in basic conditions with a transition near pH 6.[21] This redox reaction is quasi-reversible on a bare gold electrode evidenced by potential peak splitting >59 mV and asymmetry in the cathodic and anodic peak current values as shown by the CVs in Figure 1A. Nile Blue readily physisorbs

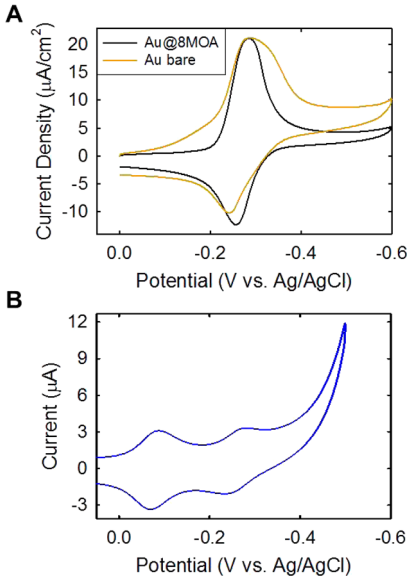

Figure 1. (A) CVs of 0.5 mM NB in 0.1 M phosphate buffer at pH 5 using a bare gold disc working electrode (gold) and a gold disc coated with a 8MOA SAM working electrode (black). (B) CV of NB tethered to a gold-coated ITO electrode via EDC/NHS coupling. The supporting electrolyte is 0.1 M phosphate buffer at pH 5. The scan rate for all voltammograms is 50 mV/s.

onto gold and silver, as seen in previous SERS electrochemical measurements,[4,6,22−24] causing a broadening of the cathodic current peak (gold curve, Figure 1A). Reduction of NB can induce desorption due to its structural change (Figure S5).[22] To prevent adsorption of NB to the gold electrode, we formed a SAM of 8MOA on a gold disc electrode to isolate the electrochemical behavior of NB in solution (black curve, Figure 1A). In this case, the CV shows one cathodic and one anodic peak consistent with previous reports.[21,27]

Next, the electrochemical behavior of NB tethered to a gold electrode was measured by covalently attaching NB to a 100 nm gold film supported by an ITO electrode using EDC/NHS coupling. In this case, the CV showed a distinct new character: two cathodic and two anodic peaks (Figure 1B). Although several reports have studied immobilized NB on electrodes, the additional peak in the voltammogram has not been discussed.[25,28−30] The appearance of new peaks at more positive potentials indicates that tethered NB undergoes two separate, energy-resolved redox reactions ($E^\circ \approx -0.060$ V and $E^\circ \approx -0.260$ V at pH 5). Each individual redox reaction shows symmetry in the cathodic and anodic peak currents indicating an improved reversibility compared to the redox reactions of solution NB. A linear dependence of peak current with scan rate confirmed that NB was successfully tethered to the gold electrode (Figure S6). Importantly, the higher energy (more negative) redox reaction of EDC/NHS coupled NB occurs approximately at the same potential as the lone redox reaction of NB in solution. We rule out 8MOA as the cause for the appearance of the lower energy redox reaction of EDC/NHS coupled NB because no current peaks are observed at this energy for the 8MOA-coated gold disc electrode used for the solution measurements in Figure 1A (Figure S7). An increase in the current negative of −0.4 V in Figure 1B is the result of the hydrogen evolution reaction from the buffer, which dominates the current at more negative potentials due to the low number of NB molecules tethered to the surface relative to the proton concentration at pH 5. In contrast, for the data in Figure 1A, the concentration of NB in solution is greater than the proton concentration at pH 5, and thus, negative of −0.4 V, the steady-state current is dominated by the diffusion-controlled reduction of NB.

Although coupling NB to a gold electrode via EDC/NHS gives rise to new electrochemical behavior, characterizing the new redox reactions with CV has limitations. The upper limit of Faradaic current that can be produced by redox reactions from NB corresponds to a monolayer of molecules. Realistically, the number of tethered NB molecules is much lower than a monolayer, especially when the relatively low and variable coupling efficiency of a primary amine to a carboxylic acid with EDC/NHS is taken into account.[31−34] Below monolayer coverages, increasing the electrode area increases not only the Faradaic current but also the capacitive background current. Thus, there is an inherent limit in the sensitivity of CV to measure EDC/NHS tethered NB redox peaks above baseline. In our experiments, we found that a majority of electrodes with tethered NB produced Faradaic current peaks only slightly above the background. Examples like those in Figure 1B were observed, but not consistently, which can be attributed to variable and low labeling using EDC/NHS coupling. To improve the Faradaic current sensitivity, we switched to characterizing the NB redox reactions with DPV. Using DPV, we were more reliably able to measure the potentials at which NB redox reactions occurred, allowing us to explore the mechanism in greater detail.

Figure 2A shows DPVs from NB tethered to a 100 nm gold film on ITO by 8MOA and EDC/NHS. As with the CV in Figure 1B, we are able to clearly resolve two individual redox reactions, which is different from the electrochemical behavior of solution phase NB. The full width at half-maximum (fwhm) for each redox peak in the CV in Figure 1B and DPVs in Figure 2A are approximately 90 mV each, suggesting that the number of electrons transferred is one.[35] It is important to point out that DPV is a differential current measurement and that bulk NB redox reactions are dependent on both electron and proton transfer. The consequence of these facts is that the cathodic and anodic peaks do not align at the same energy, as observed with simpler redox probes such as ferrocene-based molecules that only involve a single-electron transfer reaction. To rule out intermolecular interactions as a reason for the peak splitting in the DPVs, we lowered the coverage of NB by introducing a competing primary amine during the EDC/NHS coupling step in the tethering process (Figure S8). We observe that at both relatively high and low coverages, the NB redox reactions show the same potential peak splitting behavior between the cathodic and anodic waves. Further, the low NB coverage due to poor EDC/NHS coupling efficiency adds support that intermolec-

DOI: 10.1021/acs.jpcc.6b03962
J. Phys. Chem. C 2016, 120, 21091−21098

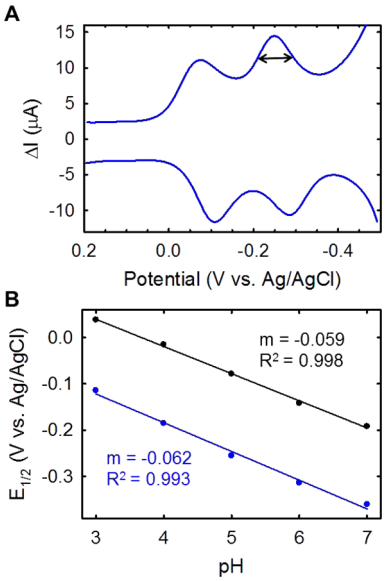

Figure 2. (A) Cathodic and anodic DPVs of NB tethered to a gold-coated electrode via EDC/NHS coupling showing two redox reactions. A 0.1 M phosphate buffer at pH 5 was used as the electrolyte. Double-sided arrow indicates an example of the fwhm at 90 mV. (B) Half-wave potential of the two redox reactions of NB tethered to a gold-coated ITO electrode via EDC/NHS coupling as the pH of the phosphate buffer is varied.

ular interactions are not responsible for the observed peak splitting behavior. An alternative explanation is that the organization of the SAM may lead to populations of tethered NB molecules with different electrode−molecule distances. This possibility was ruled out as a major contributor due to the reproducibility of peak splitting as well as the fact that we allow our SAM to form over 48 h, which permits relatively good alignment of the SAM.[36] Moreover, our calculated surface coverage suggests a low defect density.[37] Finally, as previously discussed with the solution-based NB measurements, the NB redox reaction is quasi-reversible and could play a role in the potential peak splitting.

In order to probe the mechanism behind the newly observed NB peaks, we measured the half-wave potential ($E_{1/2}$) of each redox reaction as a function of buffer pH. Figure 2B shows that the $E_{1/2}$ for each reaction (black and blue curves) is linearly dependent on pH. This result has two noteworthy implications. First, the pH dependence confirms that protons are involved in each redox reaction. Second, a linear dependence indicates that the number of protons in each reaction is constant at the range of pH values investigated. The latter result is another deviation from reported solution-based electrochemical measurements of NB, where the redox reaction switches from two protons to one proton as the pH increases past ∼6.[21] Each slope in Figure 2B closely follows the Nernstian behavior of 59 mV/pH, indicating that the number of electrons and protons are equal in each redox reaction. Adding this relationship to the ∼90 mV fwhm, we assign each redox reaction to a one proton and one electron transfer reaction. Therefore, we hypothesize that by covalently attaching NB to a gold electrode via the NHS/EDC coupling, the two proton and two electron redox reaction observed from NB in solution is split into two individual, energy-resolved redox reactions.

To identify the two individual one-proton, one-electron redox reactions of covalently immobilized NB, we compared the electrochemical response of NB to a structurally similar molecule, Cresyl Violet, using DPV. Figure 3A shows the

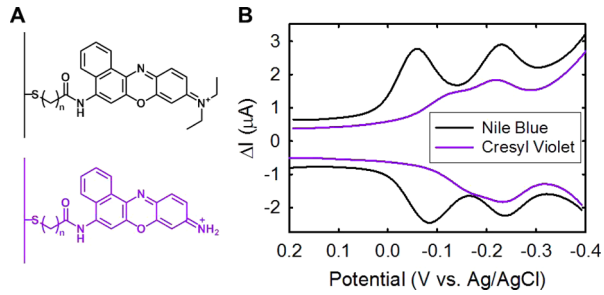

Figure 3. (A) Structure of NB (black) and Cresyl Violet (violet) when tethered to a gold surface with 11-mercaptoundecanoic acid and EDC/NHS coupling. (B) DPVs of NB (black) and Cresyl Violet (violet) tethered to a gold-coated ITO electrode as in (A) in a 0.1 M phosphate buffer at pH 5.

structure of NB (black) and Cresyl Violet (violet) after immobilization on a gold surface with EDC/NHS coupling. As drawn, the only structural difference between these two molecules is the terminal amine, with NB having a tertiary amine and Cresyl Violet a primary amine. While Cresyl Violet has two primary amines at either end of the molecule when dissolved in solution, which allows the possibility of its structure in Figure 3A to be flipped, we chose the present illustration for easier visual comparison with NB.

Regardless of the orientation of Cresyl Violet, the structural similarity between these two molecules is expected to give a similar DPV response. Interestingly, the DPV of Cresyl Violet tethered to gold in Figure 3B shows a shoulder positive of the largest peak in both the cathodic and anodic waves. As with NB, Cresyl Violet shows only one cathodic and anodic peak in solution (Figure S9) and the emergence of a shoulder when the molecule is tethered suggests a shift in energy of an underlying redox reaction. The Cresyl Violet $E_{1/2}$ has a linear dependence on buffer pH when tethered to a gold electrode (Figure S10), similar to NB. Comparing the DPV of NB and Cresyl Violet (Figure 3B), the most negative differential current peak occurs at approximately the same potential between the two molecules (∼ −0.230 V). Therefore, we tentatively assign the structurally common phenoxazine ring redox reaction (electrochemical protonation/deprotonation of the nitrogen) to the more negative potential peaks and the terminal amine redox reaction (electrochemical protonation/deprotonation) to the more positive peaks in the DPVs of each molecule. The terminal tertiary amine should be more basic than the primary amine, supporting the more positive shift in the amine redox reaction of NB compared to that of Cresyl Violet.

To further support the origin of the two NB redox reactions, we measured SERS spectroelectrochemistry of NB tethered to gold island films. As mentioned in the introduction, NB has a change in its SERS signal as it is electrochemically modulated between its oxidized and reduced forms. In order to measure how the new redox reaction impacts the SERS response of the NB, we simultaneously collect SERS spectra (Figure 4A) and SERS images (Figure 4B) of NB as the potential is swept across both redox reactions. For the spectra, we target the 590 cm^{-1} mode of NB, which has been ascribed to a ring deformation incorporating the nitrogen of the phenoxazine ring.[23,38] In the fully oxidized form of the molecule, the 590 cm^{-1} mode is strong under 642 nm laser excitation due to a resonance from

DOI: 10.1021/acs.jpcc.6b03962
J. Phys. Chem. C 2016, 120, 21091−21098

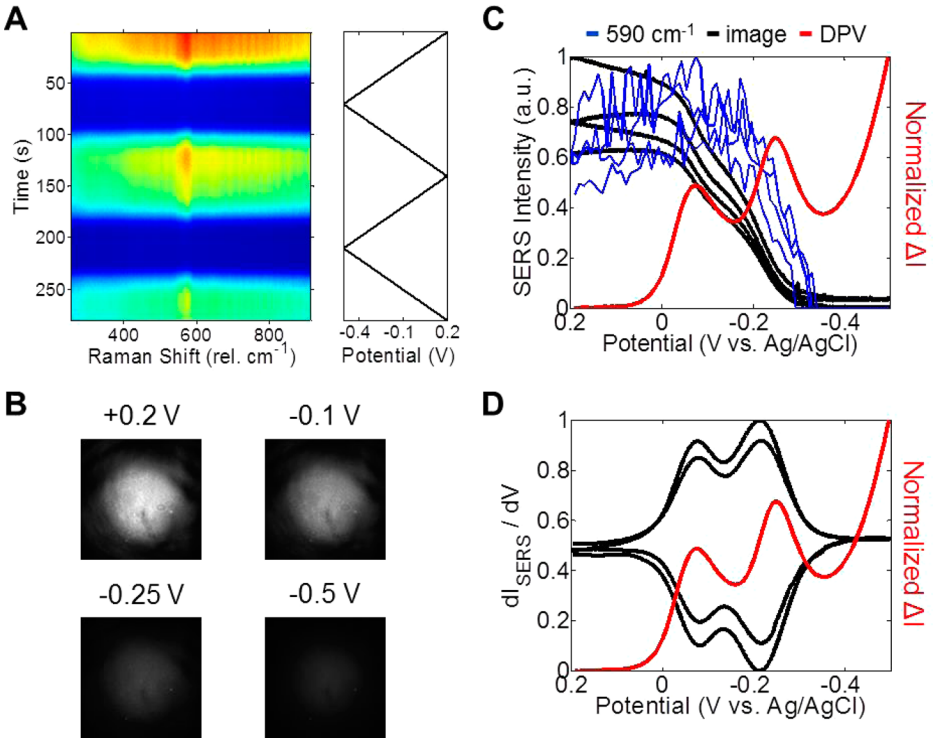

Figure 4. NB spectroelectrochemical response when tethered to an ITO-supported gold island film with EDC/NHS coupling. (A) Plot of NB SERS spectral intensity (color scale) as a function of time/applied potential and Raman shift. (B) Wide-field optical images of NB SERS from an illuminated region of the electrode surface at select potentials. (C) SERS CVs constructed from the integrated intensity of the 590 cm^{-1} spectral mode (blue) and integrated intensity of a region of interest of the optical images containing all spectral frequencies (black). Scan rate is 10 mV/s. (D) First derivative of the optical image SERS CV in (C) with respect to applied potential (black). A cathodic DPV (red) is included in (C) and (D) for comparison. All measurements were made with a 0.1 M phosphate buffer at pH 5.

the delocalized electrons across the molecule. In the fully reduced form, a break in the conjugation of the molecule shifts the electronic resonance away from the excitation energy, resulting in loss of signal from the 590 cm^{-1} mode. Figure 4A shows a spectral waterfall plot centered on the 590 cm^{-1} mode as a function of applied potential. The total spectral intensity (SERS and small background fluorescence) is high at positive, oxidizing potentials and low at more negative, reducing potentials.

High labeling densities (achieved by physisorption or solution-phase NB) show additional NB spectral features,[21] but with our electrodes and labeling strategy, there typically is only enough signal to observe the strongest 590 cm^{-1} mode. To improve our signal for monitoring the changes in SERS with electrochemical perturbation, we collect SERS images as we sweep the potential across the full NB redox window (Figure 4B). Unlike spectral acquisitions, the integrated SERS images represent all of the SERS frequencies, along with any fluorescent background emission from NB. Therefore, any SERS image intensity changes report on the entire molecule, and they should be sensitive to both the phenoxazine and terminal amine redox reactions. By collecting spectra and images simultaneously, the change in signal of NB caused by the electrochemical reaction at the phenoxazine moiety can be isolated, leaving the amine redox reaction responsible for any remaining intensity changes.

Figure 4C shows the integrated area of the 590 cm^{-1} SERS peak (blue curve) and the integrated image intensity (black curve) from the SERS images as a function of potential, allowing us to create SERS CVs. For comparison, we also overlay the cathodic DPV scan (red curve). The 590 cm^{-1} SERS CV shows a single inflection point as the intensity rises and falls in response to the applied potential, which overlaps well with the more negative potential peak in the DPV. This overlap agrees with the previous conclusion that the more negative redox reaction is associated with the phenoxazine moiety, based on the data shown in Figure 3. The SERS image CV, on the other hand, shows two inflection points, both of which overlap with the individual redox peaks in the DPV (the decrease in the maximum SERS signal over the two potential cycles can be attributed to photobleaching of NB). To better visualize these inflections, Figure 4D shows the derivative of the SERS image intensity with respect to applied potential (spectral derivative shown in Figure S11). From this, it is clear that the differential current peaks from DPV align well with the differential SERS signal. Thus, a SERS derivative plot can serve as an optical analogue to DPV. We can deduce that the more positive inflection points in the image SERS CV and DPV data are due to a redox reaction that does not directly involve the phenoxazine, because the intensity of the 590 cm^{-1} mode is relatively constant in this potential range. This is consistent with the structure analysis in Figure 3, where the more positive redox reaction was assigned to the electrochemical protonation/deprotonation of the terminal tertiary amine.

To explain the emergence of the two peaks, the structure of tethered NB (Figure 3A) needs to be taken into consideration. EDC/NHS coupling of a carboxylic acid and a primary amine leads to the formation of an amide. Considering the case of reduction, we hypothesize that the electron-withdrawing power of the carbonyl allows the first electrochemical electron

DOI: 10.1021/acs.jpcc.6b03962
J. Phys. Chem. C 2016, 120, 21091−21098

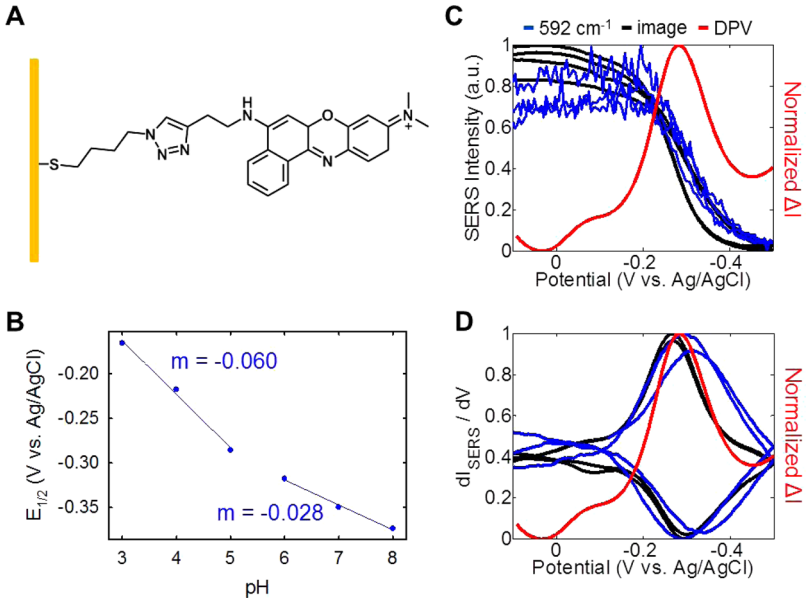

Figure 5. Spectroelectrochemistry of NB tethered to a gold-coated electrode via click coupling. (A) Structure of NB immobilized on a gold surface after azide-alkyne click chemistry. (B) Half-wave potential of the NB redox reaction as the pH of the phosphate buffer is varied. (C) SERS CVs constructed from the integrated intensity of the 592 cm^{-1} spectral mode (blue) and integrated intensity of optical images containing all spectral frequencies (black). Scan rate is 10 mV/s and the electrolyte is 0.1 M phosphate buffer at pH 5. (D) First derivative of the SERS CVs in (C) with respect to applied potential. A cathodic DPV (red) is included in (C) and (D) for comparison.

addition to be more easily incorporated by the NB molecule, shifting the redox potential to a more positive value. The opposite holds for the oxidation case. The charge of NB must be conserved after each redox reaction due to the addition of an electron and proton, which necessitates that the intermediate redox state is a radical cation. If we fit the 590 cm^{-1} peak to a Lorentzian function to extract the peak frequency and width, we do not observe appreciable changes in either of these parameters as we move from the intermediate radical cation to the fully oxidized form of the molecule (Figure S12) limiting our insight into any structural changes associated with the radical cation intermediate, although we expect the fully oxidized and fully reduced forms to resemble the solution-phase states of the molecule (Figure S13).

To test the hypothesis that the electron-withdrawing power of the amide linker helps to incorporate electron addition and thus a shift in redox reaction energy, we investigated NB tethered to a gold surface using azide−alkyne click coupling. One significant advantage of using click chemistry to tether NB to gold is that the reaction is much more quantitative and selective than EDC/NHS coupling, resulting in much higher labeling densities. Figure 5A shows the structure of NB tethered to a gold electrode via click coupling. This structure no longer has the amide linkage, but instead, it has a triazole linkage. Importantly, the triazole is electronically isolated from the NB conjugated system and therefore is not expected to alter the electrochemistry. The DPV reveals that there is one prominent cathodic and anodic peak for NB tethered in this manner (Figure S14). The differential current peak's fwhm is broadened to ∼130 mV, which indicates that the two individual redox reactions observed with EDC/NHS coupled NB are now overlapping in energy. The small positive shoulder in the DPV was determined to be unrelated to NB due to a lack of spectral response at its potential (see below for further discussion). Measuring $E_{1/2}$ as a function of buffer pH using DPV (Figure 5B) shows two linear regions—one with a slope of 60 mV/pH in acidic conditions and one with a slope of 28 mV/pH in more basic conditions—that is nearly identical to NB in solution. This response suggests a two-proton, two-electron redox reaction at pH values < ∼5.5 and a one-proton, two-electron redox reaction at pH values > ∼5.5.

Using NB tethered to a gold island film via click chemistry, we again interrogate the spectroelectrochemical response both with SERS spectra and images. A slight shift in the prominent phenoxazine mode from 590 cm^{-1} (EDC/NHS) to 592 cm^{-1} (click) was observed (Figures S12 and S15). The SERS CVs in Figure 5C show that the image intensity containing all spectral frequencies and the 592 cm^{-1} spectral mode have only one inflection point, which overlap well with the strongest DPV peak (Figure 5D). Although NB is covalently immobilized on a gold electrode, the spectroelectrochemical response is very similar to that of bulk, solution-phase NB, supporting the hypothesis that an electron-withdrawing moiety, such as the amide formed in the NHS/EDC coupling reaction, can sufficiently perturb the electron distribution in NB, inducing a shift in the energy of its redox reactions.

CONCLUSION

In summary, we used DPV and SERS spectroelectrochemistry to characterize NB electrochemistry when covalently immobilized on gold electrodes using two different attachment strategies. In the case of NHS/EDC coupling, two redox reactions were observed, each involving a single proton and electron transfer. Structural comparison with a Cresyl Violet analogue, along with simultaneous SERS image and spectral collection, allow assignment of the more positive redox reaction to the electrochemical (de)protonation of the terminal amine and the more negative redox reaction to the electrochemical (de)protonation of the phenoxazine nitrogen. The electron-withdrawing power of the amide formed in EDC/NHS coupling was hypothesized to shift the terminal amine redox reaction to lower energies. This hypothesis was further

DOI: 10.1021/acs.jpcc.6b03962
J. Phys. Chem. C 2016, 120, 21091−21098

supported by comparing the DPV and SERS data from NHS/EDC coupled NB to a triazole-linked NB formed via click chemistry, which showed redox behavior consistent with solution-phase and adsorbed NB. Interestingly, by immobilizing NB with EDC/NHS, we are able to achieve a simpler electrochemical reaction compared to physisorbed or solution-phase NB, which is advantageous in addressing nanoelectrochemical phenomena using optical probes.

■ ASSOCIATED CONTENT

Supporting Information

The Supporting Information is available free of charge on the ACS Publications website at DOI: 10.1021/acs.jpcc.6b03962.

Sulfuric acid potential cycling, 8MOA electrochemical desorption, DPV potential waveform, spectroelectrochemical cell, additional CVs and DPVs of NB and Cresyl Violet, current vs scan rate, $E_{1/2}$ of Cresyl Violet with pH, NB structures, click tethered NB SERS spectra, fit spectral frequencies and widths (PDF)

■ AUTHOR INFORMATION

Corresponding Author

*E-mail: kwillets@temple.edu. Phone: 215-204-7990.

Author Contributions

The manuscript was written through contributions of all authors. All authors have given approval to the final version of the manuscript.

Funding

Work was supported by the Department of Energy (DOE), Office of Science, Basic Energy Science (BES) under Award No. DE-SC0010307 (to A.J.W.) and the AFOSR MURI Award No. FA9550-14-1-1003 (to N.Y.M.).

Notes

The authors declare no competing financial interest.

■ ACKNOWLEDGMENTS

We thank Graham Dobereiner for helpful discussions during manuscript preparation.

■ ABBREVIATIONS

NB, Nile Blue; SERS, surface-enhanced Raman scattering; ITO, indium tin oxide; 8MOA, 8-mercaptooctanoic acid; EDC, 1-ethyl-3-(3-dimethylaminopropyl)carbodiimide hydrochloride; NHS, *N*-hydroxysulfosuccinimide; CV, cyclic voltammetry; DPV, differential pulse voltammetry

■ REFERENCES

(1) Palacios, R. E.; Fan, F.-R. F.; Bard, A. J.; Barbara, P. F. Single-Molecule Spectroelectrochemistry (SMS-EC). *J. Am. Chem. Soc.* **2006**, *128*, 9028−9029.

(2) Lei, C.; Hu, D.; Ackerman, E. J. Single-Molecule Fluorescence Spectroelectrochemistry of Cresyl Violet. *Chem. Commun.* **2008**, *43*, 5490−5492.

(3) Novo, C.; Funston, A. M.; Gooding, A. K.; Mulvaney, P. Electrochemical Charging of Single Gold Nanorods. *J. Am. Chem. Soc.* **2009**, *131*, 14664−14666.

(4) Cortés, E.; Etchegoin, P. G.; Le Ru, E. C.; Fainstein, A.; Vela, M. E.; Salvarezza, R. C. Monitoring the Electrochemistry of Single Molecules by Surface-Enhanced Raman Spectroscopy. *J. Am. Chem. Soc.* **2010**, *132*, 18034−18037.

(5) Salverda, J. M.; Patil, A. V.; Mizzon, G.; Kuznetsova, S.; Zauner, G.; Akkilic, N.; Canters, G. W.; Davis, J. J.; Heering, H. A.; Aartsma, T. J. Fluorescent Cyclic Voltammetry of Immobilized Azurin: Direct Observation of Thermodynamic and Kinetic Heterogeneity. *Angew. Chem., Int. Ed.* **2010**, *49*, 5776−5779.

(6) Wilson, A. J.; Willets, K. A. Visualizing Site-Specific Redox Potentials on the Surface of Plasmonic Nanoparticle Aggregates with Superlocalization SERS Microscopy. *Nano Lett.* **2014**, *14*, 939−945.

(7) Wilson, A. J.; Marchuk, K.; Willets, K. A. Imaging Electrogenerated Chemiluminescence at Single Gold Nanowire Electrodes. *Nano Lett.* **2015**, *15*, 6110−6115.

(8) Mathwig, K.; Aartsma, T. J.; Canters, G. W.; Lemay, S. G. Nanoscale Methods for Single-Molecule Electrochemistry. *Annu. Rev. Anal. Chem.* **2014**, *7*, 383−404.

(9) Byers, C. P.; Hoener, B. S.; Chang, W.-S.; Yorulmaz, M.; Link, S.; Landes, C. F. Single-Particle Spectroscopy Reveals Heterogeneity in Electrochemical Tuning of the Localized Surface Plasmon. *J. Phys. Chem. B* **2014**, *118*, 14047−14055.

(10) Kurouski, D.; Mattei, M.; Van Duyne, R. P. Probing Redox Reactions at the Nanoscale with Electrochemical Tip-Enhanced Raman Spectroscopy. *Nano Lett.* **2015**, *15*, 7956−7962.

(11) Zaleski, S.; Cardinal, M. F.; Klingsporn, J. M.; Van Duyne, R. P. Observing Single, Heterogeneous, One-Electron Transfer Reactions. *J. Phys. Chem. C* **2015**, *119*, 28226−28234.

(12) Liu, B.; Blaszczyk, A.; Mayor, M.; Wandlowski, T. Redox-Switching in a Viologen-Type Adlayer: An Electrochemical Shell-Isolated Nanoparticle Enhanced Raman Spectroscopy Study on Au(111)-(1 × 1) Single Crystal Electrodes. *ACS Nano* **2011**, *5*, 5662−5672.

(13) Miomandre, F.; Lépicier, E.; Munteanu, S.; Galangau, O.; Audibert, J. F.; Méallet-Renault, R.; Audebert, P.; Pansu, R. B. Electrochemical Monitoring of the Fluorescence Emission of Tetrazine and Bodipy Dyes Using Total Internal Reflection Fluorescence Microscopy Coupled to Electrochemistry. *ACS Appl. Mater. Interfaces* **2011**, *3*, 690−696.

(14) Quinton, C.; Alain-Rizzo, V.; Dumas-Verdes, C.; Clavier, G.; Miomandre, F.; Audebert, P. Design of New Tetrazine−Triphenylamine Bichromophores − Fluorescent Switching by Chemical Oxidation. *Eur. J. Org. Chem.* **2012**, *2012*, 1394−1403.

(15) Nepomnyashchii, A. B.; Bard, A. J. Electrochemistry and Electrogenerated Chemiluminescence of BODIPY Dyes. *Acc. Chem. Res.* **2012**, *45*, 1844−1853.

(16) Krumova, K.; Cosa, G. Bodipy Dyes with Tunable Redox Potentials and Functional Groups for Further Tethering: Preparation, Electrochemical, and Spectroscopic Characterization. *J. Am. Chem. Soc.* **2010**, *132*, 17560−17569.

(17) Rybina, A.; Thaler, B.; Kramer, R.; Herten, D.-P. Monitoring Hydroquinone-Quinone Redox Cycling by Single Molecule Fluorescence Spectroscopy. *Phys. Chem. Chem. Phys.* **2014**, *16*, 19550−19555.

(18) Kierat, R. M.; Thaler, B. M. B.; Kramer, R. A Fluorescent Redox Sensor with Tuneable Oxidation Potential. *Bioorg. Med. Chem. Lett.* **2010**, *20*, 1457−1459.

(19) Oja, S. M.; Guerrette, J. P.; David, M. R.; Zhang, B. Fluorescence-Enabled Electrochemical Microscopy with Dihydroresorufin as a Fluorogenic Indicator. *Anal. Chem.* **2014**, *86*, 6040−6048.

(20) Etchegoin, P. G.; Le Ru, E. C. Resolving Single Molecules in Surface-Enhanced Raman Scattering Within the Inhomogeneous Broadening of Raman Peaks. *Anal. Chem.* **2010**, *82*, 2888−2892.

(21) Ni, F.; Feng, H.; Gorton, L.; Cotton, T. M. Electrochemical and SERS Studies of Chemically Modified Electrodes: Nile Blue A, a Mediator for NADH Oxidation. *Langmuir* **1990**, *6*, 66−73.

(22) Cortés, E.; Etchegoin, P. G.; Le Ru, E. C.; Fainstein, A.; Vela, M. E.; Salvarezza, R. C. Strong Correlation Between Molecular Configurations and Charge-Transfer Processes Probed at the Single-Molecule Level by Surface-Enhanced Raman Scattering. *J. Am. Chem. Soc.* **2013**, *135*, 2809−2815.

(23) Zong, C.; Chen, C.-J.; Zhang, M.; Wu, D.-Y.; Ren, B. Transient Electrochemical Surface-Enhanced Raman Spectroscopy: A Millisecond Time-Resolved Study of an Electrochemical Redox Process. *J. Am. Chem. Soc.* **2015**, *137*, 11768−11774.

(24) Weber, M. L.; Wilson, A. J.; Willets, K. A. Characterizing the Spatial Dependence of Redox Chemistry on Plasmonic Nanoparticle Electrodes Using Correlated Super-Resolution Surface-Enhanced Raman Scattering Imaging and Electron Microscopy. *J. Phys. Chem. C* **2015**, *119*, 18591−18601.
(25) Liu, H.-H.; Lu, J.-L.; Zhang, M.; Pang, D.-W. Electrochemical Properties of Nile Blue Covalently Immobilized on Self-Assembled Thiol-Monolayer Modified Gold Electrodes. *Anal. Sci.* **2002**, *18*, 1339−1344.
(26) Walczak, M. M.; Popenoe, D. D.; Deinhammer, R. S.; Lamp, B. D.; Chung, C.; Porter, M. D. Reductive Desorption of Alkanethiolate Monolayers at Gold: A Measure of Surface Coverage. *Langmuir* **1991**, *7*, 2687−2693.
(27) Ju, H.; Ye, Y.; Zhu, Y. Interaction Between Nile Blue and Immobilized Single- or Double-Stranded DNA and Its Application in Electrochemical Recognition. *Electrochim. Acta* **2005**, *50*, 1361−1367.
(28) Nazemi, Z.; Shams, E.; Amini, M. K. Covalent Modification of Glassy Carbon Electrode by Nile Blue: Preparation, Electrochemistry and Electrocatalysis. *Electrochim. Acta* **2010**, *55*, 7246−7253.
(29) Slinker, J. D.; Muren, N. B.; Renfrew, S. E.; Barton, J. K. DNA Charge Transport Over 34 Nm. *Nat. Chem.* **2011**, *3*, 230−235.
(30) Pheeney, C. G.; Barton, J. K. DNA Electrochemistry with Tethered Methylene Blue. *Langmuir* **2012**, *28*, 7063−7070.
(31) Staros, J. V.; Wright, R. W.; Swingle, D. M. Enhancement by N-Hydroxysulfosuccinimide of Water-Soluble Carbodiimide-Mediated Coupling Reactions. *Anal. Biochem.* **1986**, *156*, 220−222.
(32) Bartczak, D.; Kanaras, A. G. Preparation of Peptide-Functionalized Gold Nanoparticles Using One Pot EDC/Sulfo-NHS Coupling. *Langmuir* **2011**, *27*, 10119−10123.
(33) Fischer, M. J. E. Amine Coupling Through EDC/NHS: A Practical Approach. In *Surface Plasmon Resonance: Methods and Protocols*; Mol, J. N., Fischer, E. M. J., Eds.; Humana Press: Totowa, NJ, 2010; pp 55−73.
(34) Sam, S.; Touahir, L.; Salvador Andresa, J.; Allongue, P.; Chazalviel, J.-N.; Gouget-Laemmel, A. C.; Henry de Villeneuve, C.; Moraillon, A.; Ozanam, F.; Gabouze, N.; et al. Semiquantitative Study of the EDC/NHS Activation of Acid Terminal Groups at Modified Porous Silicon Surfaces. *Langmuir* **2010**, *26*, 809−814.
(35) Bard, A. J.; Faulkner, L. R. *Electrochemical Methods: Fundamentals and Applications*, 2nd ed.; Wiley: New York, NY, 2001.
(36) Love, J. C.; Estroff, L. A.; Kriebel, J. K.; Nuzzo, R. G.; Whitesides, G. M. Self-Assembled Monolayers of Thiolates on Metals as a Form of Nanotechnology. *Chem. Rev.* **2005**, *105*, 1103−1170.
(37) Anandan, V.; Gangadharan, R.; Zhang, G. Role of SAM Chain Length in Enhancing the Sensitivity of Nanopillar Modified Electrodes for Glucose Detection. *Sensors* **2009**, *9*, 1295−1305.
(38) Miller, S. K.; Baiker, A.; Meier, M.; Wokaun, A. Surface-Enhanced Raman Scattering and the Preparation of Copper Substrates for Catalytic Studies. *J. Chem. Soc., Faraday Trans. 1* **1984**, *80*, 1305−1312.

DOI: 10.1021/acs.jpcc.6b03962
J. Phys. Chem. C 2016, 120, 21091−21098